Scientia Iranica D (2014) 21(3), 885–897

Sharif University of Technology
Scientia Iranica
Transactions D: Computer Science & Engineering and Electrical Engineering
www.scientiairanica.com

An efficient technique for controlling power flow in a single stage grid-connected photovoltaic system

A. Datta[a,*], G. Bhattacharya[b], D. Mukherjee[c] and H. Saha[d]

a. *Department of Electrical and Electronics Engineering, National Institute of Technology Meghalaya, Laitumkhrah, Shillong-793003, India.*
b. *Department of Physics, Ramakrishna Mission Vidyamandira, Belur Math, Howrah-711202, India.*
c. *Department of Electronics and Tele-communications Engineering, Bengal Engineering and Science University, Shibpur, Howrah-711103, India.*
d. *Centre of Excellence for Green Energy and Sensor Systems, Bengal Engineering and Science University, Shibpur, Howrah-711103, India.*

Received 20 December 2012; received in revised form 23 September 2013; accepted 15 October 2013

KEYWORDS
Single stage;
Grid-connected PV system;
Efficient technique;
Power sharing;
Automatic algorithm.

Abstract. Compared to multistage grid-connected photovoltaic systems (GCPVSs), complexity in monitoring and controlling scheme in a single-stage GCPVS is much increased, as maximum power point tracking and power sharing with the grid need to be considered simultaneously in the same stage. An efficient technique for performing the aforementioned functions, simultaneously, in a single stage system, by adjustment of the voltage phasor of a voltage source inverter, is presented. Active and reactive powers flow from the inverter is regulated by the adjustment of amplitude and phase angle of the inverter output voltage with respect to the grid voltage.

An algorithm is also developed for automatic active and reactive powers sharing for the intended applications in the single stage GCPVSs. A typical 2.8 kWp, 368 V (DC) nominal photovoltaic array based GCPVS is modeled and simulated to analyze proper load matching for different ambient and grid voltage conditions. Performances, like the efficiency of the inverter and the total harmonic distortion of the inverter output voltage and current, are studied, with variations in ambient conditions and the modulation index of a sinusoidal pulse width modulation of the IGBT based inverter. Simulation results have been included to show the feasibility of the proposed technique.

1. Introduction

The continuing decline of the cost of the photovoltaic (PV) modules, along with the advancement of power electronic and semiconductor technology, is the major factor for the widespread installation of grid-connected photovoltaic systems (GCPVSs) in recent years. The Current-Voltage ($I-V$) and Power-Voltage ($P-V$) characteristics of PV modules are nonlinear, and vary with solar insolation, ambient temperature and output voltage [1,2]. There is a unique point on the $P-V$ characteristic, called Maximum Power Point (MPP), at which PV array produces its maximum power output [3]. An appropriate Maximum Power Point Tracking (MPPT) method maintains the PV array's operating point at its MPP [1,3]. One advantageous feature of GCPVS is that they do not need battery back-ups to ensure MPPT [4].

*. *Corresponding author. Tel: +91 364 2501294; Fax: +91 364 2501113*
E-mail addresses: datta_asim@rediffmail.com (A. Datta); g_bhattacharya_2002@yahoo.com (G. Bhattacharya); dipankarm@rediffmail.com (D. Mukherjee); sahahiran@gmail.com (H. Saha)

GCPVSs are broadly classified as multi-stage systems and single-stage systems [5]. Multi-stage systems usually employ two stages. The first stage comprises a boost or buck-boost type DC/DC converter with one of its tasks being the application of the appropriate DC voltage on the PV array so that it operates at the MPP; and the second stage comprises a DC/AC inverter [6-8]. Multistage GCPVSs are in frequent use, but suffer from drawbacks of higher part counts, larger size and lower efficiency, etc. [4]. In the single stage, only a single power electronic stage between the PV array and the grid performs all the functions, namely, the electrical MPPT, boosting and inversion leading to a compact system [9,10].

Most of the conventional GCPVSs include a transformer which supports operation at low level PV array voltage input for the inverter and isolates the energy source from the utility grid. Systems including a transformer either use a line frequency or a high frequency transformer. Line frequency transformers are generally avoided due to increased size, weight and price [11]. Systems with high frequency transformers include several power stages and are pretty complex. To avoid a transformer, a single stage system has to configure high PV voltage with a string of series connected modules to make voltage output compatible with the grid interface [12].

Recent research reveals that uncontrolled PV systems connected to an electrical grid can have an adverse affect on the normal behavior of the system [13,14]. Voltage rises beyond the limits when the PV production is high and the load demand is low. Extensive voltage distortion is caused by distorted PV current under weak insolation conditions [15]. The islanding operation of the PV system may occur during the loss of utility supply after the occurrence of a fault [16]. The need for voltage regulators and phase balancers can be eliminated by properly introducing PV systems into the electricity grid, reducing, in that way, the capital and maintenance costs [15,17]. Clearly, a study on the impact of penetrating PV systems is important, and an appropriate controlling algorithm is required to avoid the unwanted consequences of the large deployment of PV systems [18,19].

The reactive power causes voltage and current loading in AC circuits, but does not result in average (active) power consumption, and is, in fact, an important component in all AC power networks [19]. The reactive power is essential for creating the needed coupling fields for AC energy-coupling devices (e.g., transformers, AC motors and generators). But excessive amounts of reactive power can overload the AC generators, causing voltage rise or fall, with reference to rated voltage in the transmission system, and can lead to collapsing the system [20]. To make transmission networks operate within desired voltage limits, methods of making up or taking away reactive power (hereafter, called reactive power control), are required [20-22]. Different approaches such as reactive power compensation and phase shifting have been applied to increase the stability and security of the power systems [18,23].

Inverters are the key element of GCPVSs which do not only transfer the DC power of the PV array to the AC grid, but also realize the MPPT function, so that the system yields maximum electricity power [5,9-11]. The majority of inverters that are currently used in GCPVS are Current Source Inverters (CSI), operating with a unity power factor, which indicates that they are capable of providing only active power to the grid system [7-10,24]. Thus, the reactive power required by the system is supplied by the reactive power compensator (e.g., shunt compensator, series compensator, FACTS controller, etc.) installed at the primary distribution system or at the substation [20,21,25]. When the insolation is weak, such CSI based systems lose their power-sharing capacity and the electrical grid has to supply directly to all loads. However, if the Voltage Source Inverter (VSI) is used instead of the CSI, reactive power can be supplied/absorbed under weak insolation condition, also, in accordance with the requirement of the grid.

This paper presents an efficient technique for a single stage GCPVS to compensate the reactive power and, simultaneously, to share the active power with the grid. The reactive power compensation and active power sharing are based on the adjustment of magnitude and phase angle of inverter output voltage with respect to the grid voltage. Inverter voltage magnitude is changed by varying the Modulation Index (MI) ($0 < m < 1$) of the Sinusoidal Pulse Width Modulation (SPWM) and the phase angle is adjusted by varying the starting instant of SPWM with respect to the zero-crossing of the grid voltage. An algorithm is also developed for execution in the controller of the inverter (e.g., dsPIC [26]) to regulate load sharing automatically based on the proposed technique of power sharing. A MATLAB/Simulink based model is developed for a 2.8 kWp, 368 V (DC) nominal PV array based single stage GCPVS to analyze the feasibility of the proposed technique and algorithm.

2. System description

The proposed GCPVS is realized using a string of series connected modules followed by an H-bridge inverter. The output of the inverter and grid are separated by a reactance, X_g. As the power output of the inverter oscillates at twice the line frequency [7,27], C_{dc} is a DC buffer capacitor across the H-bridge inverter. D is the reverse current blocking diode. Inductor L_f and

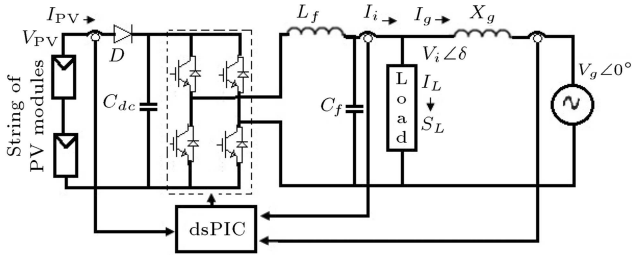

Figure 1. Schematic circuit of a single stage GCPVS.

capacitor C_f form low-pass filter in the output of the inverter. The system is synchronized with the grid and depicted in Figure 1.

Selection of different system components is as follows.

2.1. DC-link capacitor (C_{dc})

C_{dc} can be calculated using the expression [28]:

$$C_{dc} = \frac{P_{pv.n}}{2.\Delta V_{\%\text{rip}.pv}.V^2_{\min .pv}2.\pi.f_i}, \tag{1}$$

where $P_{pv.n}$ is the nominal PV array output power, $\Delta V_{\%\text{rip}.pv}$ is the percentage of the ripple in the PV array output voltage, $V_{\min .pv}$ is the minimum allowable PV array output voltage, and f_i is the grid fundamental frequency.

2.2. AC filter capacitor (C_f)

C_f can be calculated using the expression [29]:

$$C_f = \frac{1}{4.\pi^2.f_c^2.L_f}, \tag{2}$$

where f_c is the allowable cut-off frequency of the low-pass filter of the inverter.

2.3. Filter inductor (L_f)

L_f can be calculated using the expression [29]:

$$L_f = \frac{V_{i.rms}.\Delta I}{f_{sw}.\Delta I_i}, \tag{3}$$

where $V_{i.rms}$ is the rms value of inverter output voltage, ΔI is the ripple instant factor depending on minimum allowable MI of SPWM, f_{sw} is the frequency of SPWM, and ΔI_i is the allowable ripple in the inverter output current.

2.4. Grid connecting inductor (L_g)

The value of L_g can be calculated from Eq. (12) as:

$$L_g = \frac{V_{i.\max .p}.V_{g.n}.\sin\delta_{\max}}{P_{g.\max}.2.\pi.f_i}, \tag{4}$$

where $V_{i.\max .p}$ is the inverter output voltage corresponding to maximum active power transfer, $V_{g.n}$ is the rated grid voltage, and $\delta_{\max}$ is the allowable maximum phase angle.

3. System analysis

Solar PV modules must be connected in series-parallel combinations to match the required voltage and current ratings. The $I-V$ equation for an array formed by $N_{se} \times N_{pa}$ identical modules is [2]:

$$I = I_{\text{PV}}.N_{pa} - I_0.N_{pa} \cdot \left[\exp\left(\frac{V + R_s.\left(\frac{N_{se}}{N_{pa}}\right).I}{V_t.a.N_{se}} - 1\right)\right] - \frac{V + R_s.\left(\frac{N_{se}}{N_{pa}}\right).I}{R_p.\left(\frac{N_{se}}{N_{pa}}\right)}, \tag{5}$$

where I_{PV} and I_0 are the photovoltaic and saturation currents, respectively, of a PV module. R_s and R_p are the equivalent series and parallel resistances, respectively, of a module. V_t is the thermal voltage of the module, and 'a' is the diode ideality constant.

The output characteristics of solar PV array depend on the solar insolation and ambient temperature. The photovoltaic current of the solar cell can be expressed by the following equation [2]:

$$I_{\text{PV}} = (I_{\text{PV.STC}} + K_I.\Delta T).\frac{G}{G_{\text{STC}}}, \tag{6}$$

where G_{STC} and $I_{\text{PV.STC}}$ are insolation and light-generated current, respectively, under Standard Test Conditions (STC); K_I is the short circuit current temperature co-efficient; $\Delta T = T - T_n$ (T and T_n being the actual and nominal temperatures, respectively); and G is the actual insolation.

The DC output of the PV array is variable with solar insolation and temperature, and is expressed as [30]:

$$P_{dc}(t) = P_{\text{STC}}.\frac{G(t)}{G_{\text{STC}}}.[1 - \alpha.\Delta T], \tag{7}$$

where $P_{dc}(t)$ is the available DC power at any time t. P_{STC} is the maximum output at STC. 'α' is a co-efficient that expresses the power reduction due to the temperature rise of the PV array.

The amplitude of the fundamental component of the inverter output voltage is:

$$V_{1i} = m.V_{pv}, \tag{8}$$

where m is the MI of SPWM.

The simplified circuit diagram of the GCPVS is shown in Figure 2, where $V_g\langle 0°$ is the grid voltage phasor (reference), and $V_i\langle\delta$ is the inverter output voltage.

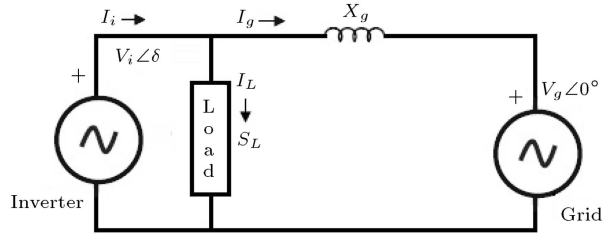

Figure 2. Simplified circuit diagram of the GCPVS.

Current from the inverter to the grid through X_g is:

$$I_g = \frac{V_i\angle\delta - V_g\angle 0}{X_g\angle 90°}. \tag{9}$$

Arrow directions in Figure 2 are the assumed positive directions of the currents.

Apparent power transferred from the inverter to the grid is [26]:

$$S_g = P_g + jQ_g = V_i\angle\delta.I_g^*, \tag{10}$$

where P_g and Q_g are the active and reactive powers, respectively, transferred from the inverter to the grid.

$$P_g - jQ_g = V_i\angle\delta^*.I_g = V_i\angle -\delta.\frac{V_i\angle\delta - V_g\angle 0}{X_g\angle 90°}. \tag{11}$$

Separating real and imaginary parts from Eq. (11):

$$P_g = \frac{V_i.V_g}{X_g}.\sin\delta, \tag{12}$$

$$Q_g = \frac{V_i^2}{X_g} - \frac{V_i.V_g}{X_g}.\cos\delta. \tag{13}$$

If $S_L(= P_L + jQ_L)$ is the load connected directly to the output terminal of the inverter, the inverter output power is:

$$S_i = P_i + jQ_i = (P_g + P_L) + j(Q_g + Q_L). \tag{14}$$

4. Inverter power losses and efficiency

Solar inverters are composed of power-electronics devices and different passive elements. Losses associated with system components and harmonics generation due to nonlinear characteristics of semiconductor devices, mainly affect the performance of the inverter. Total losses in the inverter, including losses in all passive elements, are the sum of losses incurred in its individual components [31]:

$$P_{\text{loss.total}} = P_{sw} + P_{\text{anti.diode}} + P_{dc.\text{cap}} + P_{\text{filter.ind}} + P_{\text{filter.cap}} + P_{\text{grid.ind}}, \tag{15}$$

where:

P_{sw} = power losses in switches;
$P_{\text{anti.diode}}$ = power losses in anti-parallel diodes;
$P_{dc.\text{cap}}$ = power losses in DC-link capacitor;
$P_{\text{filter.ind}}$ = power losses in filter inductor;
$P_{\text{filter.cap}}$ = power losses in filter capacitor;
$P_{\text{grid.ind}}$ = power losses in grid connecting inductor.

4.1. IGBT and anti-parallel diode losses

Losses in any semiconductor component involve conduction losses and switching losses. The conduction losses depend on the magnitude of the inverter output current, and switching losses depend mostly on the switching frequency of power switches.

4.1.1. Conduction losses (P_{con})

Conduction losses are losses due to the device's DC electrical characteristics. The conduction losses depend on current through the device and the device's DC electrical characteristics.

If the inverter output current is perfectly sinusoidal, instantaneous inverter output current (i), the duty ratios for active-stage devices (d_a) and zero-stage devices (d_z) are expressed as [32]:

$$i(t) = I_m\sin(\omega t), \qquad d_a(t) = m\sin(\omega t),$$
$$d_z(t) = 1 - m\sin(\omega t), \tag{16}$$

where I_m is the peak inverter current, ω is the angular frequency of the inverter output current, and m is the MI of SPWM.

The conduction loss of IGBT ($P_{\text{con.igbt}}$) and the conduction loss of the anti-parallel diode ($P_{\text{con.diode}}$) are computed as [32]:

$$P_{\text{con.igbt}} = \frac{1}{2\pi}\int_0^{\pi} v_{\text{CE}}(t)i_C(t)d_a(t)d\omega t = I_m v_{\text{CE0}}\frac{m}{4} + I_m^2 r_C\frac{2m}{3\pi}, \tag{17}$$

$$P_{\text{con.diode}} = \frac{1}{2\pi}\int_0^{\pi} i(t)v_D(t)i_D(t)(1 - m\sin(\omega t))d\omega t = I_m v_{D0}\left(\frac{1}{\pi} - \frac{m}{4}\right) + I_m^2 r_D\left(\frac{1}{4} - \frac{2m}{3\pi}\right), \tag{18}$$

where $v_{\text{CE}}(t)$ is the instantaneous collector-emitter voltage; $i_C(t)$ is the instantaneous collector current; v_{CE0} represents IGBT on-state zero-current collector-emitter voltage; r_C represents collector-emitter on-state resistance; $v_D(t)$ and $i_D(t)$ are instantaneous voltage across the diode and diode current, respectively; v_{D0} is the diode on-state zero-current voltage; and r_D is the diode on resistance.

4.1.2. Switching losses (P_{sw})
Switching losses depend on switching frequency, the current through the device, and the device's dynamic characteristics.

Turn-on duration of IGBT is the sum of rise time (t_r) and reverse recovery time (t_{rr}) for the free-wheeling diode [33,34].

Turn-on energy of IGBT:

$$E_{\text{IGBT\_on}} = \int_0^{t_r+t_{rr}} v_{ce}(t)i_c(t)dt. \tag{19}$$

Turn-off duration of IGBT is the sum of turn-off delay time (t_d), fall time (t_f), and tail time (t_{tail}).

Turn-off energy of IGBT:

$$E_{\text{IGBT\_off}} = \int_0^{t_d+t_f+t_{\text{tail}}} v_{ce}(t)i_c(t)dt. \tag{20}$$

Switching losses in IGBT are the product of switching energies and the switching frequency (f_{sw}):

$$P_{sw.igbt} = (E_{\text{on}.igbt} + E_{\text{off}.igbt}).f_{sw}. \tag{21}$$

Switching losses of the anti-parallel diode can be calculated as for IGBT. The turn-off loss of the anti-parallel diode due to reverse recovery, can be approximated as [34]:

$$P_{\text{diode\_off}} = \frac{1}{4}Q_{rr}V_r f_{sw}, \tag{22}$$

where Q_{rr} is the reverse recovery charge, and V_R is the reverse blocking voltage.

In modern fast recovery diodes used with IGBTs, the turn-on loss is negligible (less than 1%) compared to the turn-off loss [33].

4.2. DC-link capacitor losses

The DC-link capacitor losses depend on the equivalent series resistance (R_{ESR}) value of capacitance, and charge and discharge currents through the capacitor. If $I_{\text{ch}.rms}$ and $I_{dc.rms}$ are the charge and discharge currents through the capacitor, respectively, power loss in the capacitor is [31]:

$$P_{dc.\text{cap.loss}} = ({I_{ch.rms}}^2 + {I_{dc.rms}}^2).R_{\text{ESR}}. \tag{23}$$

4.3. AC filter capacitor losses

Dielectric loss of an AC capacitor depends on equivalent series resistance (R_{ESR}) and the frequency of the current through it. Dielectric loss of the AC filter capacitor of the inverter is:

$$P_{ac.\text{cap.loss}} = I_i^2 R_{\text{ESR}} = \frac{I_i^2.PF}{2\pi f_i.C_f}, \tag{24}$$

where I_i is the rms current through the capacitor, and PF and C_f are the power factor and capacitance, respectively, of the capacitor.

4.4. Filter and grid connecting inductor losses

The rms value of the inductor current is [34]:

$$I_{L\_rms} = \sqrt{I_{dc}^2 + I_{ac}^2} \approx \sqrt{I_i^2 + \frac{\Delta I_i^2}{12}}, \tag{25}$$

where I_{ac} is the AC inductor current, I_{dc} is the DC inductor current, I_{ac} is the AC inductor current, I_i is the RMS value of the fundamental inverter output current, and ΔI_i is the inverter output current ripple.

Power losses in an inductor are $P_{\text{loss.Ind}} = P_{\text{core}}$ (core loss) + P_{dcr} (wire loss caused by DC resistance) + P_{acr} (wire loss caused by AC resistance). These losses can be expressed as:

$$P_{\text{core}} = k.f_g^{\alpha}.b^{\beta}.V_e, \qquad P_{dcr} = I_{dc}^2.R_{dc.\text{ind}},$$
$$P_{acr} = I_{ac}^2.R_{ac.\text{ind}}, \tag{26}$$

where, k is a constant for core material and depends on core material, b is the peak flux density, α is frequency exponent, β is flux density exponent, V_e is effective core volume, and $R_{dc.\text{ind}}$ and $R_{ac.\text{ind}}$ are the DC and AC resistances of the inductor, respectively.

Losses in the grid connecting inductance (L_g) can be calculated using the same expressions used for filter inductor losses.

The efficiency of a solar inverter is not constant, as power losses consist of a constant part and a load-dependent part [30]. The constant part includes the power needed for control circuitry, IGBT drivers and other auxiliary parts of the inverter. Moreover, core losses in the passive components of the inverter are included in the constant part, as voltage variation in a solar inverter is small compared to the current. The load-dependent part includes all current dependent losses in the passive components of the inverter, the conduction and the switching losses in the power switches (e.g., IGBT) of the inverter. The load independent part of the inverter losses, in terms of percentage of inverter nominal power, is given by [35]:

$$P_0 = \frac{1}{99}.\left(\frac{10}{\eta_{10}} - \frac{1}{\eta_{100}} - 9\right), \tag{27}$$

where η_{10} and η_{100} are the efficiencies at 10% and 100% of the inverter nominal power.

Power losses of the inverter, in terms of the percentage of nominal power, are given by:

$$P_{\text{inv.loss}} = P_0 + k.P^2, \tag{28}$$

where:

$$k = \frac{1}{\eta_{100}} - P_0 - 1, \qquad P = \frac{P_{\text{inv.out}}}{P_{\text{inv.rated}}}. \tag{29}$$

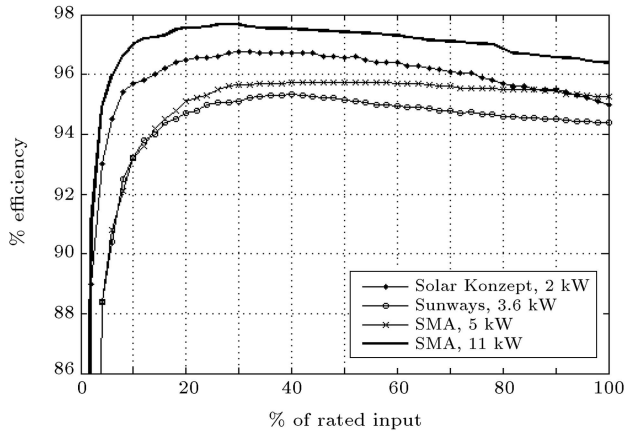

Figure 3. Efficiency of various solar inverters as a function of the percentage rated DC power: (a) Solar Konzept, 2 kW; (b) Sunways, 3.6 kW; (c) SMA, 5 kW; and (d) SMA, 11 kW.

Table 1. P_0 and k of the efficiency curves.

Inverters	η_{10} (%)	η_{100} (%)	P_0	k
Solar Konzept, 2 kW	95.6	95	0.0041	0.0485
Sunways, 3.6 kW	93.4	94.4	0.0065	0.0528
SMA, 5 kW	93.4	95.2	0.0066	0.0438
SMA, 11 kW	97	96.3	0.0027	0.0357

$P_{\text{inv.out}}$ is the inverter output power at a particular ambient conditions, and $P_{\text{inv.rated}}$ is the rated power of the inverter.

Therefore, inverter efficiency is expressed as:

$$\eta_{\text{inv}} = \frac{P}{P + P_0 + k.P^2}. \tag{30}$$

The efficiency curves of various solar inverters as a function of percentage rated DC power are shown in Figure 3. Table 1 shows P_0 and k of the efficiency curves in Figure 3.

An inverter with relatively low power, during sunrise and sunset or during cloudy days, will operate at low efficiency. On the other hand, an inverter with relatively large power will lead to a waste of energy when the available PV array power is larger than its rated power [30,35].

5. Harmonic distortion

Harmonic currents generated by the PV systems downgrade the quality of the electrical grid and alter the performance of other electrical equipment. Harmonic distortion in inverter output voltage or current is associated with: the switching mechanism in semiconductor devices, variation of solar insolation and variation of grid frequency [36]. Compared to voltage harmonics, current harmonics are strongly dependent on the fluctuations of insolation [37]. The high current distortion observed at the low power input of the inverter implies the inability of the control circuit and sensors to measure and maintain the sinusoidal shape waveform of the output current [38]. Generally, the effect of harmonics is not so prominent at low concentrations of PV systems, but the situation may get worse as the PV capacity increases.

The individual harmonic distortion for current at the kth harmonic order is given by [38]:

$$\text{HDI}_k = \frac{I_k}{I_1}, \tag{31}$$

where, I_k is the rms value of the kth harmonic order component and I_1 is the fundamental component of the inverter output current.

Total Harmonic Distortion (THD) in inverter output current is expressed as:

$$\text{THD}_I = \sqrt{\sum_{k=2}^{n} \text{HDI}_k^2}, \tag{32}$$

where n is the highest harmonic order.

Similar expressions for harmonic distortions are also valid for inverter output voltage.

As per the IEEE standard 519-1992 [39], the maximum allowable THD for the consumer (voltage and current) must be limited to 5%. The maximum individual harmonic components must be limited to 3% for voltage lower than 69 kV.

6. Reactive power compensation and active power sharing

At any value of δ, active and reactive powers supplied by the inverter are balanced by the active and reactive powers drawn by the load and grid. Neglecting conductor and leakage losses, as per the active and reactive powers balance principle, separate equations are: $P_i + P_L + P_g = 0$ and $Q_i + Q_L + Q_g = 0$. Variations of active and reactive powers sharing with the variation of δ for a constant connected load of $500\langle 0°$ VA in the range of δ, $-30°$ to $+30°$, are depicted in Figure 4.

The concept of load sharing/balancing is with the following conventions:

- Supplied active power is positive and consumed/received active power is negative.
- For the inverter and transmission line, absorbing reactive power (inductive) is positive and supplying reactive power (capacitive) is negative.
- For load, inductive reactive power is negative and capacitive reactive power is positive.

Referring to Figure 4, active power supplied by the

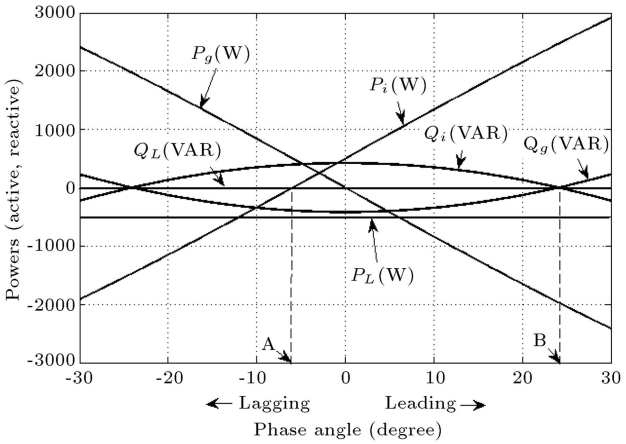

Figure 4. Variations of active and reactive powers with phase angle (δ) for $V_i = 220$ V, $V_g = 230$ V, $X_g = 10\ \Omega$, and $S_L = 500\langle 0^\circ$ VA.

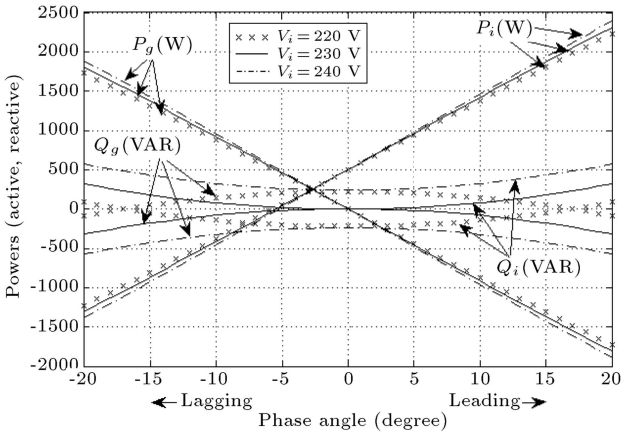

Figure 5. Active and reactive powers sharing with the variation of phase angle for $V_i = 220$ V, 230 V and 240 V with $V_g = 230$ V, $X_g = 10\ \Omega$, and $S_L = 500\langle 0^\circ$ VA.

inverter at point 'A' is zero, and, for δ less than at point 'A', the inverter active power becomes negative. As the inverter cannot draw active power, the system should not operate for δ less than at point 'A'. With the increase of δ from 'A' (towards the leading side), the active power supply from the inverter gradually increases.

Inverter generates capacitive reactive power in the range of δ: 'A' to 'B'. At 'B', reactive power is zero. Further increase of δ (towards the leading side) causes generation of inductive reactive power. In other words, the inverter absorbs reactive power (inductive VAR injection) from the grid in the range of δ: 'A' to 'B', and supplies reactive power (capacitive VAR injection) in the range of δ greater than at 'B' towards the leading side.

Figure 5 shows load sharing for three different inverter voltages: $V_i = 220$ V, 230 V and 240 V, with constant grid voltage, $V_g = 230$ V. It is observed that for $V_i = 230$ V and $V_i = 240$ V (i.e., $V_i \geq V_g$), the

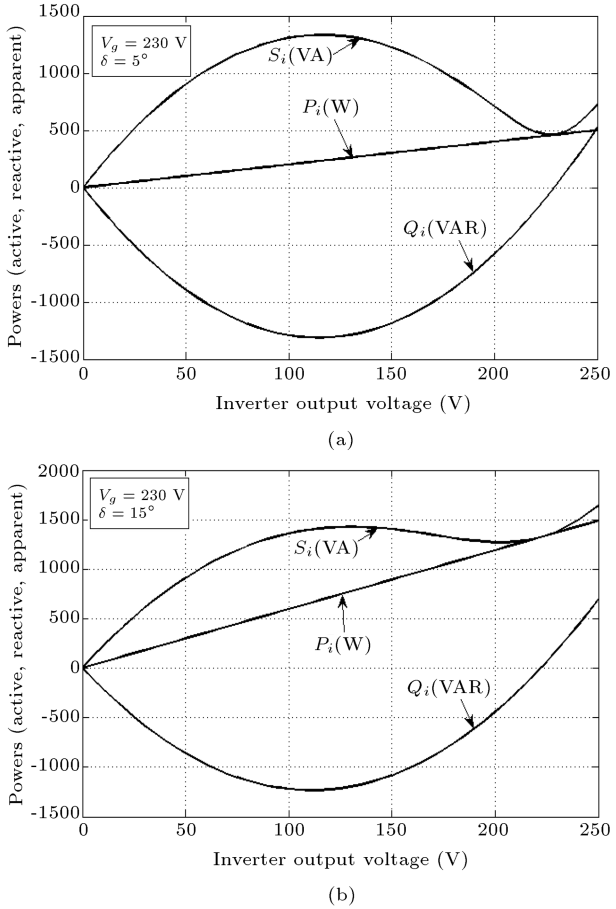

Figure 6. Variation of active and reactive powers with inverter output voltage (V_i) at (a) $\delta = 5^\circ$ and (b) $\delta = 15^\circ$ with $V_g = 230$ V and $X_g = 10\ \Omega$.

inverter injects inductive VAR and active power to the grid with the adjustment of δ. Whereas, for $V_i = 220$ V (i.e., $V_i \leq V_g$), the inverter injects capacitive VAR at low values of δ and inductive VAR at higher values of δ, with active power to the grid.

Figure 6(a) and (b) show variations of active and reactive powers supply from the inverter with variations of inverter output voltage at a constant value of δ. Reactive power supply (capacitive) is maximum at $V_i = (V_g/2).\cos\delta$ (where, $\partial Q_g/\partial V_i = 0$) and gradually decreases with the increase of V_i. Reactive power becomes zero at $V_i = V_g.\cos\delta$. Further increase of V_i causes increased reactive power (inductive) absorbtion. Thus, reactive power compensation and active power sharing in a VSI based GCPVS can be regulated by adjustment of the inverter output voltage and phase angle.

7. The proposed algorithm

Sensing parameters:

PV voltage, V_{pv},

PV current, I_{pv},

Inverter output voltage, V_i,

Grid voltage, V_g,

Distribution line current, $I_{\rm DL}$,

The signal sensing topology for the control unit of the inverter is shown in Figure 7. An algorithm is developed for power factor controlling and active power sharing, sensing the above mentioned quantities, and depicted in Figure 8.

With the change of δ at constant magnitudes of V_i and V_g, variation of reactive power is less compared to active power. Similarly, variation of active power is less compared to the variation of reactive power with the change of inverter voltage magnitude at constant δ. The algorithm is based on adjusting reactive injection/absorption by adjustment of inverter voltage magnitude first, and then adjusting active power by adjustment of δ. The MPPT function of the PV system is based on the adjustment of δ, by trial and error, for which PV array output power (P_{PV}) is maximum at a particular ambient condition.

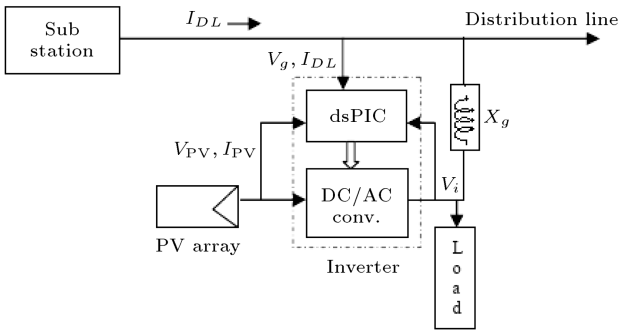

Figure 7. Signals sensing topology of the dsPIC for the proposed algorithm.

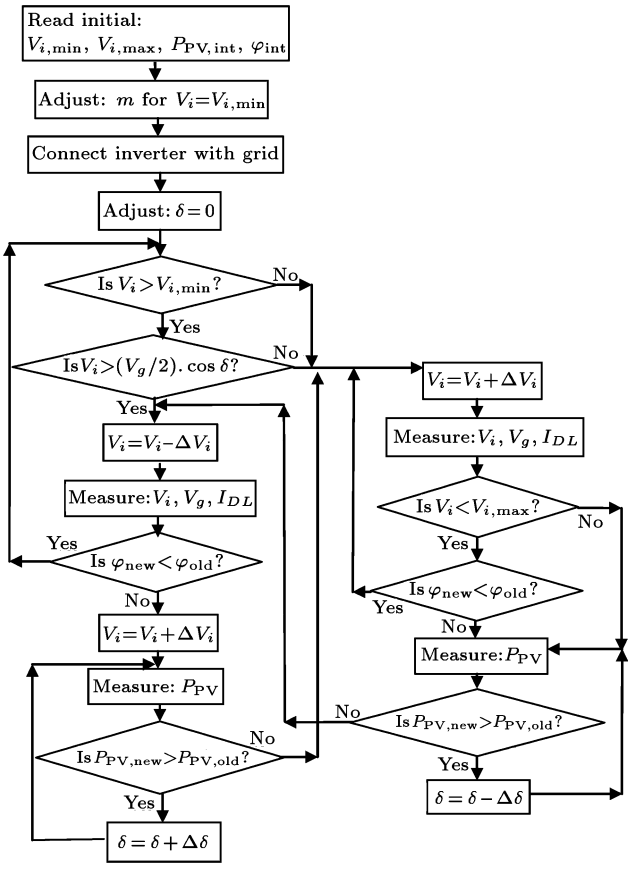

Figure 8. The proposed algorithm.

The algorithm is based, for reactive power compensation and active power sharing, by trial and error, on the following principles:

- After changing inverter voltage magnitude by a small value ($\pm\Delta V_i$), dsPIC compares $\varphi_{\rm new}$ with $\varphi_{\rm old}$ (only value not sign) and sets φ for the smaller one. φ is the phase angle between the distribution line current ($I_{\rm DL}$) and grid voltage (V_g).
- After changing δ by a small value ($\pm\Delta\delta$), dsPIC compares new PV array power ($P_{pv.\rm new}$) with previously measured PV array power ($P_{pv.\rm old}$) and sets δ always for the greater one. The dsPIC calculates PV array output power (P_{pv}) by measuring PV array output voltage (V_{pv}) and PV array output current (I_{pv}).

8. Results and discussion

A MATLAB/Simulink model for a typical 2.8 kWp, 368 V (DC) nominal PV array (14 numbers KC200GT [40] modules in a string) based GCPVS is presented in Figure 9. Values of C_{dc} (16 μF), C_f (3.2 μF), L_f (6.4 mH) and L_g (56.7 mH) are calculated for the simulation model using Eqs. (1) to (4), respectively, with: the derating factor for $P_{\rm PV.nominal}$ = 80%, the derating factor for V_i is 80%, $\Delta V_{\%\rm rip.pv}$ = 5%, $V_{\min .pv}$ = 200 V, ΔI = 0.41, ΔI_i = 10% of rated inverter output current, $\delta_{\max}$ = 40°, f_g = 50 Hz, f_{sw} = 10 kHz, and f_c = 1000 Hz. Derating factors for $P_{\rm PV}$ and V_i are used as practical working condition their values, which hardly reach rated values but are less than rated values. $I-V$ and $P-V$ characteristics of the PV array are shown in Figures 10 and 11, respectively. To justify reactive power compensation, a variable RLC (resistor-inductor-capacitor) load is connected with V_g in the simulation model and RLC load is adjusted for different $\phi_{\rm before}$ values. $\phi_{\rm before}$ is the angle between V_g and variable RLC load current before connecting the inverter with the grid. Then, the inverter is connected in parallel to the variable RLC load, as shown in the simulation model (Figure 9). A local load (S_L) is also connected directly to the inverter output terminals. Before connecting the inverter, V_g and $\phi_{\rm before}$ are adjusted for different values. After the inverter is connected for particular ambient conditions i.e. temperature (T) and insolation (G), V_i is adjusted

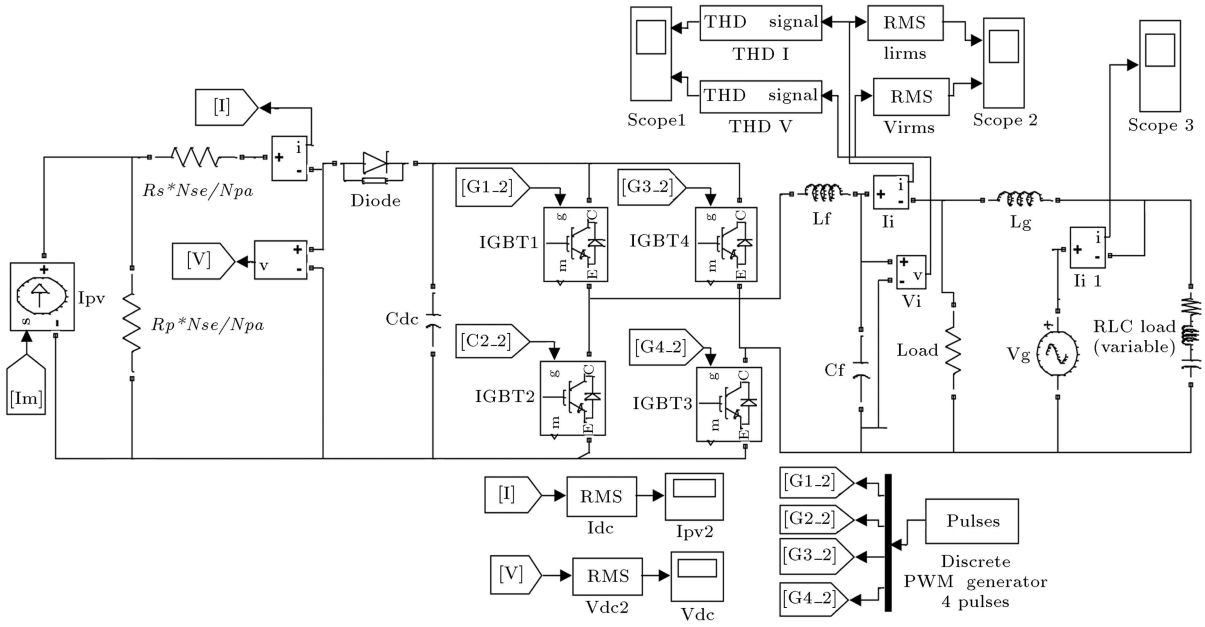

Figure 9. MATLAB/Simulink model of single stage GCPVS.

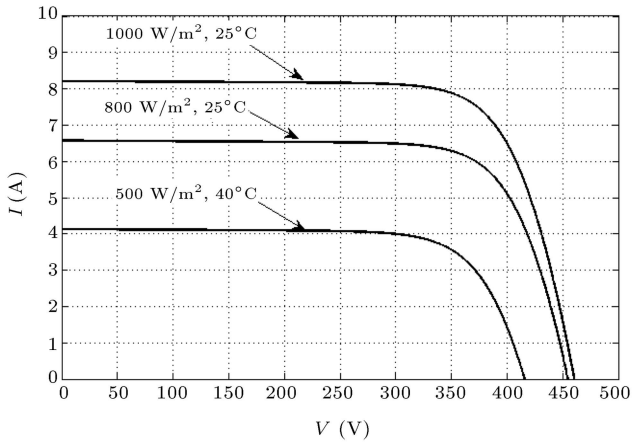

Figure 10. $I-V$ characteristics of 2.8 kWp, 368 V (DC) PV array.

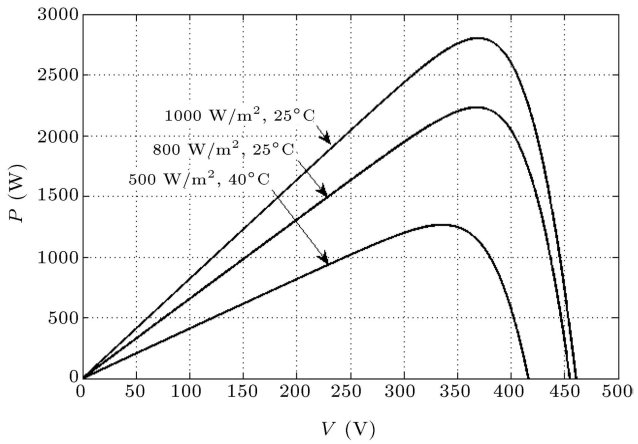

Figure 11. $P-V$ characteristics of 2.8 kWp, 368 V (DC) PV array.

for a minimum value of φ, and δ is adjusted, for which P_{PV} becomes maximum. Minimum value ($V_{i.\min}$) and maximum value ($V_{i.\max}$) of V_i are chosen to be 200 V and 235 V, respectively. The choice of $V_{i.\,\min}$ and $V_{i.\,\max}$ values are restricted mainly by the voltage tolerance of the local load connected directly to the inverter output terminals. A δ value should not occur corresponding to a negative value of inverter active power. Simulation results of reactive power compensation and active power sharing at different ambient conditions are tabulated in Table 2. V_{mpp}, P_{mpp}, V_i, δ, P_i, Q_i, P_g, Q_g, ϕ_{after}, η_{inv}, THD_v and THD_I are measured after connecting the inverter with the grid. Results show that ϕ_{after} (phase angle between V_g and variable RLC load current) values are decreased due to reactive power compensation by the inverter. The significance of positive and negative signs of active and reactive power is discussed in Section 6 of the paper. At high PV power generation, δ becomes comparatively greater to transfer large power to the grid. In this condition, the reactive power contribution from the inverter is less and active power sharing is more. But, at low PV power generation, the inverter can supply comparatively large compensating reactive power.

Figure 12 shows variation of inverter efficiency with different insolation levels at constant temperature and MIs of SPWM. As per Figure 12 and results in Table 2, the inverter efficiency is high whenever input is near the rating of the inverter, and vice versa. Inverter efficiency is higher at higher values of MI.

As per Figure 13 and results in Table 2, the THDs of the inverter output voltage and current are not constant. THD increases with the decrease of

Table 2. Simulation results at different ambient conditions.

Sl no.	1	2	3	4	5	6
Insolation (G), W/m^2	1000	1000	800	500	1100	500
Ambient temperature (T), °C	25	40	25	15	40	40
Grid voltage (V_g), V	200	210	220	230	210	235
MPP voltage (V_{mpp}), V	368	342	364	378	341	332
MPP power (P_{mpp}), W	2800	2596	2230	1437	2859	1263
Inverter output voltage (V_i), V	235	230	228	220	230	210
Phase angle (δ), Deg.	27	25	24	12	29	10
Inverter output power (S_i), VA	2602	2290	1984	1157	2684	968
Active power supplied by inverter (P_i), W	2334	2141	1913	1152	2441	856
Reactive power supplied by inverter (Q_i), VAR	1335	812	540	-109	1116	-450
Active power transferred to grid (P_g), W	-2134	-2041	-1913	-1052	-2342	-856
Reactive power transferred to grid (Q_g), VAR	-1335	-912	-540	109	-1066	450
Inverter local active load (P_L), W	-100	-100	0	-100	-100	0
Inverter local reactive load (Q_L), VAR	0	100	0	0	-50	0
Modulation index (m)	0.9	0.92	0.88	0.82	0.95	0.89
Φ_{before} ($\angle V_g, I_{DL}$), Deg. (before reactive power compensation by inverter)	-30	-15	-12	3	-25	9
Φ_{after} ($\angle V_g, I_{DL}$), Deg. (after reactive power compensation by inverter)	-12	-1	0	0	-1	3
Inverter efficiency (η_{inv}), %	93	89	91	81	100	79
THD of inverter output voltage (THD$_v$), %	3.8	4	4.5	4.7	3.7	5
THD of inverter output current (THD$_I$), %	4.6	4.6	4.9	5.1	4.4	5.3

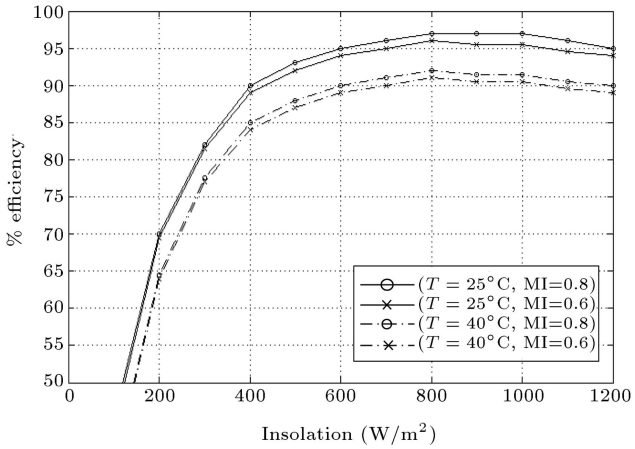

Figure 12. Variation of the inverter efficiency with the variation of insolation with SPWM at 10 kHz.

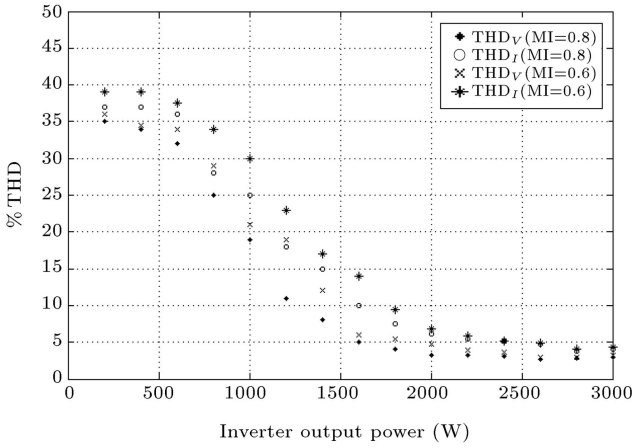

Figure 13. %THD in inverter output voltage and current with the variation of inverter output power [V_{dc} = 368 V].

PV generation. The THD of the current is greater compared to that in the voltage. In fact, for very low PV generation, THD can exceed IEEE-519 standard. At higher values of MI, the THDs of both inverter voltage and current decrease. However, over modulation of SPWM causes a significant third harmonic current component, resulting in higher THD at the grid side.

9. Conclusion

An efficient technique of reactive power compensation and active powers sharing based on the adjustment of voltage magnitude and phase angle of a VSI in a single stage GCPVS is presented. Moreover, an algorithm, based on the proposed technique, is developed for

the intended application in the single stage GCPVSs. According to the strategy, during sunlight, the PV system sends active power to the grid and, at the same time, compensates for the reactive power of the grid.

A simulation-based study is performed for the following objectives:

a) To ascertain the acceptability of the proposed technique and algorithm;

b) To ascertain the impact of penetrating PV systems into an electrical grid, so that attention can be paid to avoid all possible unwanted consequences of penetrating PV systems.

The simulated results have shown how the algorithm, based on the proposed technique, adjusted the power angle and the amplitude of the inverter voltage, and, consequently, controlled the active and reactive powers supplied to or absorbed by the grid. The results also confirmed that the proposed technique and algorithm-based system performed well for the analysed PV system.

References

1. Khan, B.H., *Non-conventional Energy Resources*, 1st Edn., pp. 117-147, Tata McGraw-Hill Publishing Company Limited, India (2006).
2. Villalva, M.G., Gazoli, J.R. and Filho, E.R. "Modeling and circuit-based simulation of photovoltaic arrays", *Brazilian Journal of Power Electronics*, **14**(1), pp. 35-45 (2009).
3. Narendiran, S. "Grid tie inverter and MPPT - A review", *Int. Conf. on Circuits, Power and Computing Tech. (ICCPCT)*, Nagercoil, India, pp. 564-567 (2013).
4. Jain, S. and Agarwal, V. "A single-stage grid connected inverter topology for solar PV systems with maximum power point tracking", *IEEE Trans. Power Electron*, **22**(5), pp. 1928-1940 (2007).
5. Xue, Y., Chang, L., Kjaer, S.B., Bordonau, J. and Shimizu, T. "Topologies of single-phase inverters for small distributed power generators: An overview", *IEEE Trans. Power Electron*, **19**(5), pp. 1305-1314 (2004).
6. Yang, B., Li, W., Zhao, Y. and He, X. "Design and analysis of a grid-connected photovoltaic power system", *IEEE Trans. on Power Electron*, **25**(4), pp. 992-1000 (2010).
7. Barbosa, P.G., Braga, H.A.C., Rodrigues, M.D.C.B. and Teixeira, E.C. "Boost current multilevel inverter and its application on single-phase grid-connected photovoltaic systems", *IEEE Trans. Power Electron*, **21**(4), pp. 1116-1124 (2006).
8. Beser, E., Arifoglu, B., Camur, S. and Beser, E.K. "A grid-connected photovoltaic power conversion system with single-phase multilevel inverter", *Sol. Energy*, **84**, pp. 2056-2067 (2010).
9. Kjaer, S.B., Pedersen, J.K. and Blaabjerg, F. "A review of single-phase grid-connected inverters for photovoltaic modules", *IEEE Trans. Ind. Appl.*, **41**(5), pp. 1292-1306 (2005).
10. Sahan, B., Vergara, A.N., Henze, N., Engler, A. and Zacharias, P. "A single stage PV module integrated converter based on a low-power current source inverter", *IEEE Trans. Ind. Electron.*, **55**(7), pp. 2602-2609 (2008).
11. Xiao, H., Xie, S., Chen, Y. and Huang, R. "An optimized transformerless photovoltaic grid-connected inverter", *EEE Trans. Ind. Electron.*, **58**(5), pp. 1887-1895 (2011).
12. Zhang, L., Sun, K., Xing, Y. and Xing, M. "H6 transformerless full-bridge pv grid-tied inverters", *IEEE Trans. Power Electron*, **29**(3), pp. 1229-1238 (2014).
13. Ai, Q., Wang, X. and He, X. "The impact of large-scale distributed generation on power grid and microgrids", *Renew. Energy*, **62**, pp. 417-423 (2014).
14. Auld, A.E., Brouwer, J., Samuelsen, G.S. "Analysis and visualization method for understanding the voltage effect of distributed energy resources on the electric power system", *Electr. Power Syst. Res.*, **82**(1), pp. 44-53 (2012).
15. Zeng, Z., Yang, H., Zhao, R. and Cheng, C. "Topologies and control strategies of multi-functional grid-connected inverters for power quality enhancement: A comprehensive review", *Renew. Sust. Energy Rev.*, **24**, pp. 223-270 (2013).
16. Ahmad, K.N.E.K., Selvaraj, J. and Rahim, N.A. "A review of the islanding detection methods in grid-connected PV inverters", *Renew. Sust. Energy Rev.*, **21**, pp. 756-766 (2013).
17. Wang, L.Y., Zhang, B.H., Wang, K.Q., Guo, Z., Zhang, G.C., Luo, S.B., Xie, H., Yu, G.L. and Xue, J. "An approximate solution to lower tap changing or capacitors regulator times in reactive power control in distribution systems", *Int. J. Electr. Power Energy Syst.*, **28**(7), pp. 491-495 (2006).
18. García, C. "Policies and institutions for grid-connected renewable energy: "Best practice" and the case of China", *Governance*, **26**(1), pp. 119-146 (2013).
19. Woyte, A., Thong, V.V., Belmans, R. and Nijs, J. "Voltage fluctuations on distribution level introduced by photovoltaic systems", *IEEE Trans. Energy Convers.*, **21**(1), pp. 202- 209 (2006).
20. Calderaroa, V., Conio, G., Galdia, V. and Piccolo, A. "Reactive power control for improving voltage profiles:

A comparison between two decentralized approaches", *Electr. Power Syst. Res.*, **83**(1), pp. 247-254 (2012).

21. Araa, A.L., Aghaeib, J., Alaleh, M. and Barati, H. "Contingency-based optimal placement of optimal unified power flow controller (OUPFC) in electrical energy transmission systems", *Scientia Iranica D*, **20**(3), pp. 778-785 (2013).

22. Amjady, N. "Voltage security monitoring of power systems by a new continuation method", *Scientia Iranica*, **9**(4), pp. 392-403 (2002).

23. Araa, A.L., Kazemib, A., Gahramania, S. and Behshad, M. "Optimal reactive power flow using multi-objective mathematical programming", *Scientia Iranica D*, **19**(6), pp. 1829-1836 (2012).

24. Albuquerque, F.L., Moraes, A.J., Guimarães, G.C., Sanhueza, S.M.R. and Vaz, A.R. "Photovoltaic solar system connected to the electric power grid operating as active power generator and reactive power compensator", *Sol. Energy*, **84**, pp. 1310-1317 (2010).

25. Aghaei, J., Gitizadeh, M. and Kaji, M. "Placement and operation strategy of FACTS devices using optimal continuous power flow", *Scientia Iranica D*, **19**(6), pp. 1683-1690 (2012).

26. Datta, A., Bhattacharya, G., Mukherjee, D. and Saha, H. "Towards stable grid voltage through load sharing in an Indian grid connected PV system", *26th European Photovoltaic Solar Energy Conf. (26th PVSEC)*, Hamburg, Germany, pp. 4205-4210 (2011).

27. Ho, B.M.T. and Chung, H.S.H. "An integrated inverter with maximum power tracking for grid-connected PV systems", *IEEE Trans. Power Electron.*, **20**(4), pp. 953-962 (2005).

28. Kjaer, S.B. "Design and control of an inverter for photovoltaic applications", Ph.D. Dissertation, Aalborg University, Denmark (2005).

29. Araújo, S.V., Zacharias, P. and Mallwitz, R. "Highly efficient single-phase transformerless inverters for grid-connected photovoltaic systems", *EEE Trans. Ind. Electron.*, **57**(9), pp. 3118-3128 (2010).

30. Demoulias, C. "A new simple analytical method for calculating the optimum inverter size in grid-connected PV plants", *Electr. Power Syst. Res.*, **80**, pp. 1197-1204 (2010).

31. Tehrani, K.A., Rasoanarivo, I. and Sargos, F.M. "Power loss calculation in two different multilevel inverter models (2DM2)", *Electr. Power Syst. Res.*, **81**, pp. 297-307 (2011).

32. Gu, B., Dominic, J., Lai, J.S., Chen C.L., LaBella, T. and Chen, B. "High reliability and efficiency single-phase transformerless inverter for grid-connected photovoltaic systems", *IEEE Trans. Power Electron.*, **28**(6), pp. 2235-2245 (2013).

33. Rajapakse, A.D., Gole, A.M. and Wilson, P.L. "Electromagnetic transients simulation models for accurate representation of switching losses and thermal performance in power electronic systems", *IEEE Trans. Power Delivery*, **20**(1), pp. 317-327 (2005).

34. Wei, W., Hongpeng, L., Jiawan, Z. and Dianguo, X. "Analysis of power losses in z-source PV grid-connected inverter", *8th Int. Conf. on Power Electronics - ECCE Asia*, The Shilla Jeju, Korea, pp. 2588-2592 (2011).

35. Notton, G., Lazarov, V. and Stoyanov, L. "Optimal sizing of a grid-connected PV system for various PV module technologies and inclinations, inverter efficiency characteristics and locations", *Renew. Energy*, **35**, pp. 541-554 (2010).

36. Batrinu, F., Chicco, G., Schlabbach, J. and Spertino, F. "Impacts of grid-connected photovoltaic plant operation on the harmonic distortion", *IEEE Mediterranean Electrotechnical Conf. (MELECON)*, Malaga, pp. 861-864 (2006).

37. Ortega, M.J., Hernández, J.C. and García, O.G. "Measurement and assessment of power quality characteristics for photovoltaic systems: Harmonics, flicker, unbalance, and slow voltage variations", *Electr. Power Syst. Res.*, **96**, pp. 23-35 (2013).

38. Andrei, H., Ulieru, V.D., Chicco, G., Cepisca, C. and Spertino, C.F. "Photovoltaic applications", *J. Mater. Process. Technol.*, **181**, pp. 267-273 (2007).

39. IEEE recommended practices and requirements for harmonic control in electrical power systems, IEEE Standard 519-1992 (1992).

40. Data sheet of KC200GT photovoltaic module. http://www.kyocerasolar.com/assets/001/5195.pdf. accessed 25.10.12).

Appendix

Parameters of KC200GT module [40] under STC are presented in Table A.1.

Table A.1. Parameters of KC200GT module under STC (25°C, 1.5 AM, 1000 W/m^2).

Maximum power current, I_{mp}	7.6 A
Maximum power voltage, V_{mp}	26.3 V
Maximum power, $P_{\max}$	200 W
Short circuit current, I_{sc}	8.2 A
Open circuit voltage, V_{oc}	32.9 V
Diode ideality constant, a	1.3
Number of cells per module, N_s	54
Temperature coefficient of V_{oc}, K_v	-0.1230 V/K
Temperature coefficient of I_{sc}, K_I	0.0032 A/K

Biographies

Asim Datta received the B.E. and M.Tech. degrees in electrical engineering from Tripura University and University of Calcutta, India, in 1999 and 2001, respectively. Currently, he is working as an Assistant Professor in the department of Electrical and Electronics Engineering, National Institute of Technology, Meghalaya, India, where as he is currently working towards the Ph.D. degree. His research interest is grid-connected photovoltaic systems and embedded systems.

Goutam Bhattacharya graduated from Calcutta University, India, in Physics. He received his M.S. and Ph.D. degrees in Physics (solar photovoltaic systems and instrumentation) from Kalyani University, India, in 1980 and 1989, respectively. He has been a lecturer under Burdwan University, and R.K.M. Vidyamandira, Calcutta University, India, where he is the head of the Department of Physics. His present fields of interest are electronic instrumentation, DSP based instrumentation and photovoltaic power converters. He is also involved in number of government projects in India.

Dipankar Mukherjee received the B.E. and M.TelE. degrees from Bengal Engineering and Science University, India, in 1974 and 1977, respectively. Later, he completed Ph.D. from Jadavpur University, India. He is professor and Ex-HOD of the department of Electronics and Tele-communications Engineering, Bengal Engineering and Science University. His principal research interest centers around the design and analysis of integrated energy systems. He is also involved in number of projects under Government of India.

Hiranmay Saha received the M.Tech. and Ph.D. degrees from Calcutta University and Jadavpur University, India, in 1967 and 1977, respectively. He was former Chairman of Solar Energy Division (Eastern Region), MNRE, Govt. of India, and advisor of WBREDA, Govt. of West Bengal. He was associated with Jadavpur University as a professor in the department of Electronics and Telecommunications Engineering. Currently, he is coordinator of Centre of Excellence for Green Energy and Sensor Systems, Bengal Engineering and Science University and Chairman of the Board of Directors of Agni Power & Electronics Pvt. Ltd., India. His main research interest is smart embedded systems, MEMS and photovoltaic systems. He is also involved in number of projects under Government of India.